Entangled Photons and Bell State Inequality

Shashank Dharanibalan[a)]

This lab report covers the use of the qutools Entanglement Demonstrator to measure an entangled quantum state called Bell State ($|\Phi\rangle$) using the polarizations of pair of entangled photons. The measurement process is called tomography and the process of measurement inherently destroys the state created using SPDC. The tomography of a single qubit results in an impure state and we lose the information of the Bell State, while the two-qubit tomography preserves the purity of the Bell State and retains useful information of the prepared state. Additionally, using two variations of the Bell State, the singlet $|\Phi^-\rangle$ and triplet state $|\Phi^+\rangle$, we can prove the presence of a quantum mechanical explanation by violation of the Bell inequality, the inequality measurement for the triplet state was $2.516 \pm 0.03 (\geq 2)$ as the state had a high visibility and a density matrix had a fidelity of 0.93. While the singlet state was $1.7 \pm 0.03 (\leq 2)$ as the state had poor visibility in the diagonal basis and a fidelity of only 0.71. Finally, the correlation function was used to show that one arm of the SPDC set-up was insufficient to match the theoretical expectation of $g^{(2)}(0) = 0$ as the photons were very "bunched" resulting in a value of 1.06 ± 0.23. However, with a fiber-based beam-splitter and the other detector arm as a trigger, the heralded correlation function matches expectations where $g_H^{(2)}(0) = 0.143 \pm 0.23$ close to 0.

Keywords: Tomography, Density, Coincidences, Entanglement, Polarization, Correlation, Fidelity, Inequality

I. INTRODUCTION: ENTANGLED PHOTON STATES

The goal of this section of the lab was to demonstrate the property of entanglement in a physical experiment not unlike the 'quantum eraser' phenomenon with the Mach-Zehnder experiment. The entangled quantum state will be demonstrated using the creation of entangled pairs of infrared photons through a non-linear crystal. This polarization of the photons will form the basis of measurement of the quantum state of these photons. The lab will demonstrate how the final polarization state of the photons will be entangled and cannot be predicted before the optics setup. The polarization basis measurements can construct a density matrix that can describe the state using quantum tomography.

II. THEORY

The process of converting polarized input light to a lower energy, higher wavelength infrared light with an entangled polarization state is called SPDC which occurs in a non-linear crystal whose orientation with another non-linear crystal in an orthogonal position will create entangled photons. A photon's state will be measured from the visibility in different polarization bases. The basis for pairs of orthogonal operations that can be represented as Bloch vectors to form the Poincaré sphere. The ability to measure the state leads to tomography which provides the density matrix of the state. The density matrix is a square Hermitian matrix that contains the probability of measuring the total state in different polarizations for each of the pair of entangled photons created via SPDC.

II.A. Polarization Basis

The measurements are conducted via projection operations of the Polarization basis. Similar to Bloch's sphere, the polarization bases are eigenstates of the X, Y, and Z Pauli matrices as seen in Figure 1. The basis $|P\rangle$ and $|M\rangle$ polarizations are the diagonal and anti-diagonal orientation while $|R\rangle$ and $|L\rangle$ are circular polarizations with opposite helicality. The diagonal basis is also written as the $|+\rangle$ and $|-\rangle$ respectively.

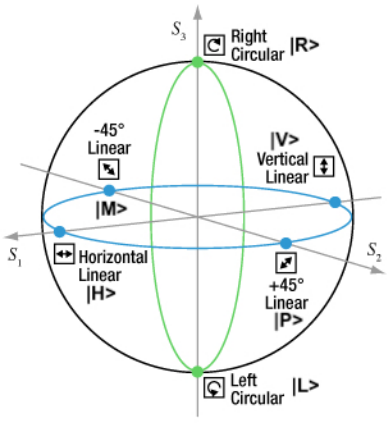

Fig. 1: Poincaré sphere of the polarization measurements. The other basis can be written in terms of $|H\rangle$ and $|V\rangle$where $|P, M\rangle = \frac{1}{\sqrt{2}}(|0\rangle \pm |1\rangle)$ and $|R, L\rangle = \frac{1}{\sqrt{2}}(|0\rangle \pm i|1\rangle)$

II.B. Spontaneous Photon Down Conversion (SPDC)

The SPDC process changes the polarization and wavelength of light as it passes through a non-linear crystal made of Barium Borate called a BBO. This process involves pumping photons into the crystal which converts the photon into a pair of photons each with half of the frequency of the pumped photon. The energy of this process is defined by the interaction Hamiltonian. Each term of the Hamiltonian contains creation and destruction operators that raise and lower the energy level of the pair of photons as seen in Eqn 1. Due to the conservation of energy, the output photons have larger wavelengths (red photons) compared to the input photons with half the wavelength as the output (blue photons)[2].

$$V = \hbar\kappa \left(a^{2\dagger} b + a^2 b^\dagger\right) \tag{1}$$

Additionally, the BBO crystal alters the polarization state of the pair of photons. The red photons are always orthogonally polarized to the input blue-pumped photons. The polarization axis of the BBO crystal determines the orthogonal orientation of the red photons along with the polarization of the input blue photons. To generate an equal amount of pairs with different polarization for entanglement, the following set-up is used called Type-I phase matching.

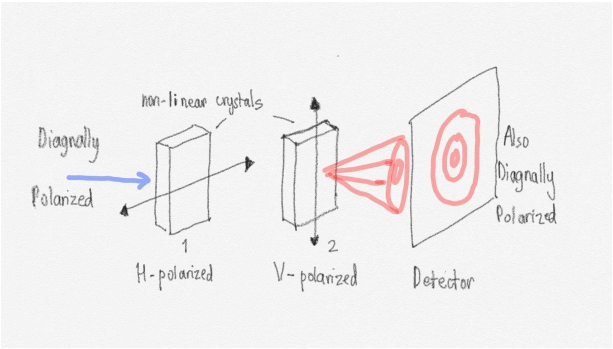

Fig. 2: Type I Phase Matching with two BBO crystals with orthogonally to each other and pumped with diagonally aligned blue photons

The construction of the set-up is with two BBO crystals that are orientated with orthogonal polarization axes to each other and are pumped with blue photons. Since each BBO crystal outputs a pair of red photons with the same polarization axis as the BBO, the input blue photons are orientated with diagonal polarization with a half-wave plate. Thus, the output red photons are also diagonally polarized, the first crystal would create a $|H_1 H_2\rangle$ and the second crystal would create a $|V_1 V_2\rangle$ state as seen from the orientation in Figure 2. Entanglement occurs from the fact that the pair of photons cannot be traced to any particular crystal, so the measurement of either polarization basis is equal, resulting in the following state seen in Eqn 2.

$$|\psi\rangle = \frac{1}{\sqrt{2}}\left[|V_1\rangle|V_2\rangle + e^{i\phi}|H_1\rangle|H_2\rangle\right] \tag{2}$$

II.C. Quantum State Tomography

II.C.1. Measurement of Polarization

The process of tomography involves measuring the counts of the state in all the polarization bases to construct a density matrix in terms of the Pauli matrices and their coefficients. The down-converted pairs of photons are split into two paths and are reflected into arms that can carry a quarter wave plate (QWP) and rotating polarizer each. The arms end with a fiber coupler that connects to a "quCR" that can display the number of photons detected in each arm. A QWP is an optical component that is orientated to measure circularly polarized light at a specific angle. Along with the rotating polarizer, Table 1 shows the arrangement of angles of the QWP and Polarizer to measure the counts in one arm for one qubit tomography[3].

Table I: Angle Orientation for different measurement basis

Polarization	QWP Angle ($\theta°$)	Pol. Angle ($\theta°$)	Counts
$\|H\rangle$	0	0	h
$\|V\rangle$	0	90	v
$\|P\rangle$	45	45	p
$\|M\rangle$	45	-45	m
$\|R\rangle$	45	90	r
$\|L\rangle$	45	0	l

Both the QWP and Polarizer in different combinations to measure the counts in different polarization bases as seen in the Poincaré Sphere. The detected counts are shown on the quCR display

Furthermore, these combinations of the angles apply to the same components in the other arm that measures the other "qubit". Therefore, when moving to two-qubit tomography, the whole state must be measured thoroughly for high accuracy and there will be a total of 36 measurements arising from the combination of the different possible bases for each qubit. The following matrix shows the visual representation of the counts for different basis combinations for two-qubit tomography.

$$\text{Counts} = \begin{pmatrix} h_1h_1 & h_1v_2 & h_1p_2 & h_1m_2 & h_1r_2 & h_1l_2 \\ v_1h_2 & v_1v_2 & v_1p_2 & v_1m_2 & v_1r_2 & v_1l_2 \\ p_1h_2 & p_1v_2 & p_1p_2 & p_1m_2 & p_1r_2 & p_1l_2 \\ m_1h_2 & m_1v_2 & m_1p_2 & m_1m_2 & m_1r_2 & m_1l_2 \\ r_1h_2 & r_1v_2 & r_1p_2 & r_1m_2 & r_1r_2 & r_1l_2 \\ l_1h_2 & l_1v_2 & l_1p_2 & l_1m_2 & l_1r_2 & l_1l_2 \end{pmatrix}$$

II.C.2. Reconstruction of the density matrix

The information on the measurements is insufficient for reliable and interpretable results by eye. The construction of a density matrix returns the information to the

Pauli matrix basis and the elements of the density matrix will contain the probability of measuring the qubit(s) in that specific basis. The general process follows the creating a coefficients matrix (T) that is in terms of Pauli basis and then finally summing up the terms to create the composite density matrix. The process for a single qubit is simpler as there is only one set of measurements as seen from Eqn 3. The base assumption is that for no polarizer or QWP (coefficient T_0), we measure a probability of 1.

$$\rho = \frac{1}{2}\sum_{s} T_s \sigma_s \tag{3}$$

The density matrix of the two-qubit state cannot be written as the tensor product between two qubits. This is because the measurements made are coupled with the polarization for each permutation of measurement. As before in the single qubit tomography, the next step is to create a coefficients matrix of size 4 x 4 matrix because they are in the Pauli bases.

$$\mathrm{T} = \begin{pmatrix} T_{00} & T_{0z} & T_{0x} & T_{0y} \\ T_{z0} & T_{zz} & T_{zx} & T_{zy} \\ T_{x0} & T_{xz} & T_{xx} & T_{xy} \\ T_{y0} & T_{yz} & T_{yx} & T_{yy} \end{pmatrix}$$

Finally, the density matrix for a two-qubit system can be generalized from Eqn 3 to get the probabilities for all the state combinations for the photon pairs incident on the fiber couplers. The density matrix for both the one-qubit and two-qubit tomography can be obtained algorithmically and is detailed in the Appendix with the sample coded function in PyThon and a run-down of the construction with a specific element of the large Counts matrix.

$$\rho = \frac{1}{4}\sum_{s_1,s_2=0}^{n} T_{s_1 s_2} \bigotimes_{j=1}^{2} \sigma_j$$

III. PROCEDURE

The procedure involves two aspects improving the calibration of the quED set-up as a whole and subsequently using a quarter wave plate and rotating polarizer to construct the density matrix using several measurements in all combinations of the basis covered in Figure 1. The use of the density matrix shows the behavior of the state with different probabilities displayed. The "quED" set-up starts with the half-wave plate which polarizes the light diagonally for photon pumping as seen in Fig 2. The BBO crystals are placed between a birefringent lens that corrects the paths of the incidentally pumped photons so there is an even entanglement between two polarization states on a given basis. Fig 3 shows the internal optical components for optimized SPDC.

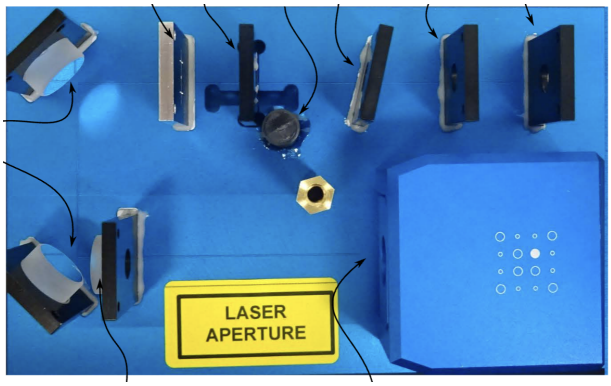

Fig. 3: The BBO crystal is located on the top right between the two birefringent compensation crystals that phase and spatially match the down-converted photons. The half-wave plate is located on the top left in the transparent casing

The main aspects of calibration are pointing alignment and beam-walking. The pointing alignment is to ensure that the beam from the pump laser is focused into the center of the fiber coupler, the process is done by iteratively adjusting only the corresponding adjuster on the fiber coupler and reflecting mirror for one arm at a time. The rotation of both adjusters must be done simultaneously in small increments to maximize the number of counts in that arm. The beam-walking is a more general process after improved counts for both arms. This is to ensure the coincidences are also maximized between both arms and is done repeatedly with the pointing-alignment in case the single counts fall for any one of the arms. Fig 4 shows the full set-up of the quED and the adjusters required for calibration for both arms.

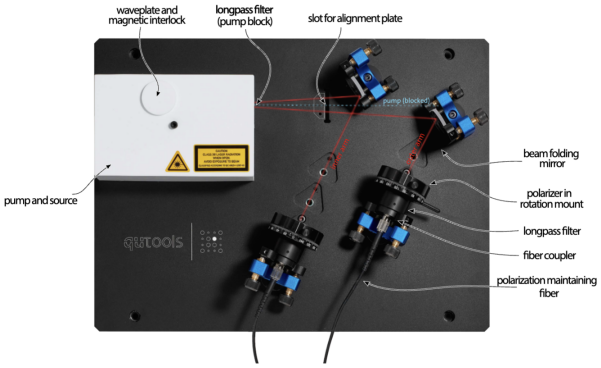

Fig. 4: The down-converted photons travel down two separate paths each with a quarter wave plate and polarizer for measurements. The arm ends with a fiber coupler that transmits the polarized light to the quCR to display counts and coincidences

IV. RESULTS AND ANALYSIS

IV.A. Operating Power of the Entanglement Demonstrator

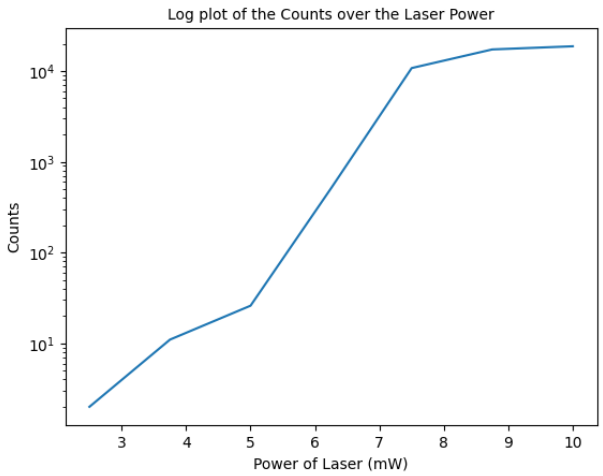

Fig. 5: Logarithmic Plot of the Counts detecting for increasing Operating Power of the laser

Fig 5 shows the logarithmic trend of the incident counts with increasing current driving the laser. The increasing power of the system means that more red photons are being downconverted and form larger energy packets that travel along the quED set-up into each detector arm and register count.

IV.B. Visibility Without Calibration

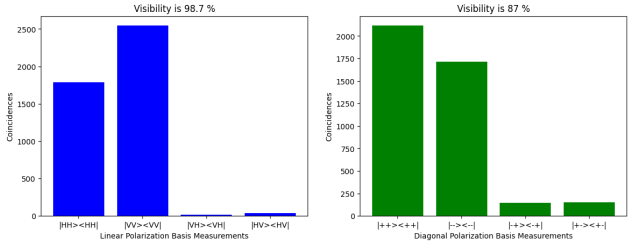

(a) Linear Basis **(b)** Diagonal Basis

Fig. 6: The plots are the counts in the linearly polarized basis and the diagonally polarized basis. The counts show that entanglement is occurring for the photon state as the counts are nearly evenly distributed indicating an equal probability of measuring in either state

Uncalibrated visibility is poor for the diagonal basis because the state is not maximally coupled and the state is imbalanced in its entangled favoring the $|VV\rangle$ measurement basis compared to the $|HH\rangle$ measurements.

IV.C. Visibility After Calibration

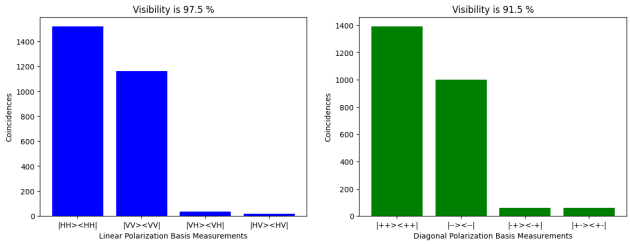

(a) Linear Basis **(b)** Diagonal Basis

Fig. 7: The calibration process improves the visibility, especially for the diagonal basis of measurement, and improves the evenness of the probability of measurement for the two states of $|\psi\rangle$

The visibility is much better after beam-walking and it evens the counts between both detectors to handle any spatial mismatching within the quED set-up, maximizing the counts for the expected basis for showing entanglement. This result shows the counts are not perfectly balanced in the basis but are nevertheless entangled to rule out any local hidden variables.

IV.D. Single Qubit Tomography

The density matrix for the following single qubit tomography is reconstructed from the single counts from one of the arms of the quED and using the Python function detailed in the appendix. The matrix contains the probability of measuring $|H\rangle$ in the top left element and the probability of measuring $|V\rangle$ state in the bottom right element, both along the diagonal.

$$\rho = \begin{pmatrix} 0.498 & 0.001j \\ 0.001j & 0.501 \end{pmatrix}$$

$$\mathrm{Tr}\,(\rho) = 1.0$$

$$\mathrm{Tr}\,(\rho^2) = 0.5$$

$$\text{Bloch Vector}\,(\vec{v}) = [-0.0014, -0.002, -0.003]$$

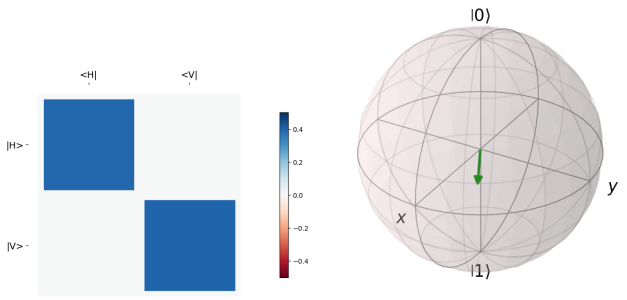

(a) Density Plot **(b)** Bloch Vector

Fig. 8: Fig a) shows the density plot as a color plot. The trace of the matrix is 1 and the purity is exactly 0.5, The tomography is conducted using the single count rate of the second detector as one of the qubits. Fig b) shows the Bloch Vector of the matrix whose magnitude is less than 1. Therefore, these two figures show that a single qubit measurement results in a mixed state

The measurement of only one of the qubits destroys the entirety of the two-qubit state and as expected from theory, also destroys entangled from any kind of "observation". As expected from our visibility calculation, the full entangled state is in the $|\Phi^+\rangle$ state. The probability of measuring $|H\rangle$ is 0.49 and 0.51 for the $|V\rangle$, which indicates an almost equal chance of being in either polarization state as expected from the initial Bell State. However, the purity of the Bell state is lost from measuring only one qubit, therefore the Purity is 0.5. It appears too convenient that the fidelities are almost even in the density matrix but it is not possible to obtain an error calculation of the fidelities or the purity because the construction of the density matrix as detailed in the theory section and the Appendix constraints and assumes that coefficient of T_0 is equal to 1. The true use of this density matrix is to illustrate how we lose "information" of our whole state. It suggests that the same one qubit density matrix could be obtained easily with a mixed and random mixed state with density matrix like $|\rho_{\text{rand}}\rangle = \frac{1}{2}|0\rangle\langle 0| + \frac{1}{2}|1\rangle\langle 1|$.

IV.E. Two Qubit Tomography

The density matrix from the 36 measurements at different configurations is seen below. This measures the entirety of the entangled state constructed by the polarization of the pairs of photons created via SPDC. The measurement destroys the state but as seen below, it captures all the information we need to completely describe the type of entanglement.

$$\begin{pmatrix} 0.45 & 0.03{+}0.03i & -0.01{+}0.03i & 0.43{-}0.16i \\ 0.03{-}0.03i & 0 & 0 & 0.02{-}0.03i \\ -0.01{-}0.03i & 0 & 0.011 & -0.03{-}0.03i \\ 0.43{+}0.16i & 0.02{+}0.03i & -0.03{+}0.03i & 0.54 \end{pmatrix}$$

$\text{Tr}(\rho) = 1.0$

$\text{Tr}(\rho^2) = 0.935$

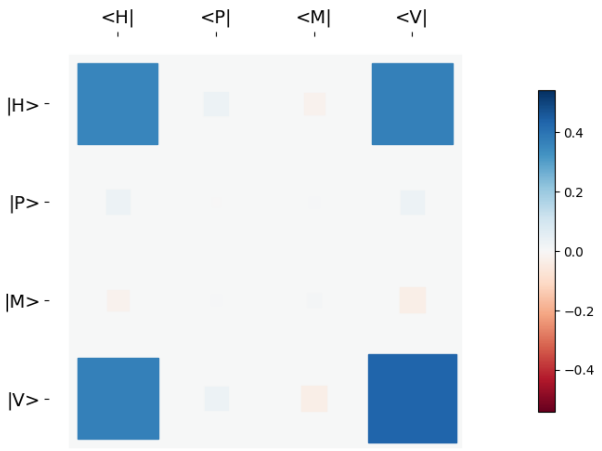

Fig. 9: The visualized density plot from two-qubit tomography matches the theoretical expectation of the density matrix $\rho_t = |\psi\rangle\langle\psi|$. The tool of Fidelity shows that this state is around 93% similar to our theoretical state in Eqn 2.

Similar to the one qubit tomography case, the trace of the density matrix is 1, assuring that the reconstruction algorithm is written correctly. Additionally, the purity of the density matrix is almost 1, assuring us that the initial state was indeed pure and only measuring both photon states gets us a pure density matrix. The purity should ideally be 1, but as the density plot shows, the initialization of the state was not ideal and we do not have perfect fidelity in the $|\Phi^+\rangle$ as expected. The lobsided density plot indicates more pumped blue photons entering the BBO crystal were phase-matched spatially and temporally for the vertically polarized state than the horizontal state, therefore the resulting entanglement is not balanced perfectly between horizontal and vertical polarization for both qubits.

V. INTRODUCTION: BELL STATE INEQUALITY

VI. THEORY

In this section of the lab, the quantum nature of light is investigated more closely by considering the lowest energy packet of light as an indivisible photon. The measurements made in tandem with the tomography tools described earlier will help us discern if we are investigating our created entangled state with the quantum behavior with some local hidden variable in the classical sense. The two states that are dealt with is the Singlet state $|\psi_s\rangle = |\Phi^-\rangle = \frac{1}{\sqrt{2}}[|H_1H_2\rangle - |V_1V_2\rangle]$ and the Triplet state $\psi_t\rangle = |\Phi^+\rangle = \frac{1}{\sqrt{2}}[|H_1H_2\rangle + |V_1V_2\rangle$.

VI.A. Detection of SPDC photons

The down-converted photons from the crystal arrive in pairs into two beam "arms" with fiber couplers that

are detected by silicon photodiode detectors. The detectors only register single detection events (a photon at a time) and in a given detection window (Δt_w), a coincidence is detected if both photons are detected in both detectors within this window. To rule out properties of the detector and to only investigate the particle nature of light, Hanbury Twiss-Brown devised an experiment to measure coincidences by placing a fiber-based beam-splitter on the fiber-coupled arms of the set-up to show that for the lowest energy, a photon in the fiber cannot be divided and will travel by either the transmitted path or the reflected path of the beam-splitter. Therefore, a coincidence detection will not be possible as the photon can be detected in only one of the detectors on the outputs of the beam-splitter[1].

$$g^{(2)}(\tau = 0) = \frac{N_{01}}{N_0 N_1} \frac{T}{\Delta t_w} \tag{4}$$

To quantify the results of this hypothesis, the second-order correlation function is devised to consider the probabilities of measuring coincidences given a probability of single detections. The subscript in the equation indicates the counts detected for a connected channel on the detector. N_{01} is the counts registered when detections are made in both channels 0 and 1 within the time window. N_0 and N_1 are respectively counts registered for single detections in each of the channels. For the HBT set-up described so far, the following equation describes the correlation function for $\tau = 0$. The expectation is that for a classical regime, a coherent source of light will result in $g^{(2)}(0) \geq 1$ as the light is traveling as a light will register multiple coincidences when it is both transmitted and reflected by the beam-splitter. While for the quantum regime, where light is a stream of single photons the result is $g^{(2)}(0) < 1$. Within the quantum regime, if $g^{(2)}(0) = 0$ then the stream of photons is spaced apart and is not detected one after the other, called anti-bunching. For random photon emissions, $g^{(2)}(0) = 1$ and is said to be bunching photons as it is on the cusp of the quantized regime.

Specifically for the SPDC photon source, the heralded second-order correlation function must be used. The "heralded" phrase comes from the fact the SPDC source produces a pair of photons that are entangled so a photon detected in one arm automatically informs us that another photon in the other arm must be detected. To illustrate this experimentally Fig ? shows the types of coincidences we are dealing with between the heralded and non-heralded case. For the general HBT set-up, only 2-fold coincidence counts are considered as there are only two outputs from the beam splitter, in our heralded case, we can be doubly sure of our counts registered because it considers 3-fold coincidences where the first channel (Channel 0) is the "trigger" arm without a beam-splitter and the other two channels (1 and 2) are the outputs of the beam-splitter that is connected to the second heralded arm. The following equation is an analog to Equation ? and is different as the detections are now conditioned by the trigger arm detections.

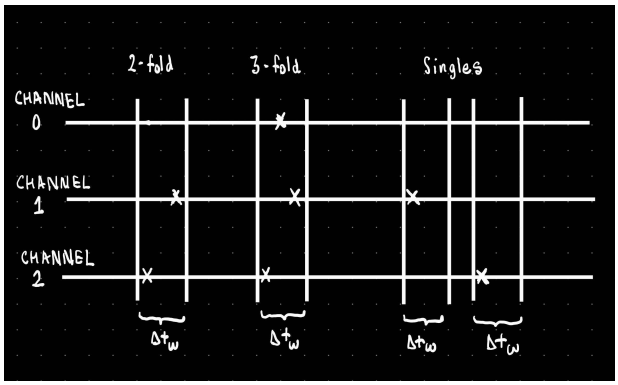

Fig. 10: This figure shows the coincidence logic and time window for each channel where coincidences are detected. Two detections between two channels is a 2-fold coincidence. If there are three detections, it is a 3-fold coincidence. Detections that occur beyond the time window across channels are only single detection events

$$g_H^{(2)}(\tau = 0) = \frac{N_{012} N_0}{N_{01} N_{02}} \tag{5}$$

VI.B. CHSH-Bell Inequality

This experiment's goal is to ascertain not only the quantum mechanical theory of light but also to rule out any local hidden variables that can be explained via classical explanations. The key idea proposed by Clauser, Horne, Shimony, and Holt (where CHSH comes from) is that classical correlations between a set of measurements made by two observers of our system result in an absolute value of ≤ 2 while the quantum mechanical theory predicts a larger correlation that is maximized at $\leq 2\sqrt{2}$. For the case of our Singlet and Triplet states of the photon polarization, the observables are the probabilities of measuring counts in various pairs of polarization settings for the pair of polarizers (act as the observers). Eqn 6 is the Bell Inequality for the Singlet state that shows the classical bounds for the sum of the correlations. The angles $\alpha\,(\alpha')$ and $\beta\,(\beta')$ are the four combinations of angles for each of the polarizers on each of our arms to measure the coincidences of the entangled state[4].

$$S = E_1(\alpha, \beta) + E_2(\alpha', \beta) - E_3(\alpha, \beta') + E_4(\alpha', \beta') \leq 2 \tag{6}$$

$$E(a, b) = \frac{N(a, b) - N(a, b_\perp) - N(a_\perp, b) + N(a_\perp, b_\perp)}{N(a, b) - N(a, b_\perp) + N(a_\perp, b) + N(a_\perp, b_\perp)} \tag{7}$$

$$\Delta S = \sqrt{\left(\sum_{\alpha, \alpha' = 0} \sum_{\beta, \beta'} \Delta E(a, b)^2 \right)} \tag{8}$$

The perpendicular notation signifies that the angle of the polarizer is rotated 90 degrees to its perpendicular location for all the combinations of coincidence measurements. Additionally, the specific choices of angles will affect the CHSH Inequality measurement even if all the choices lead to a violation. From the Equation above we can infer that for maximum violation of the CHSH inequality, the coincidence counts need to have a contrast

between the first and last measurement for each of the four E. Therefore, the E_S expectations negative sign in the summation, to make the $\langle S \rangle$ maximum. The experimental method will show a different maximization of the triplet state ($|\Phi^+\rangle$).

VII. PROCEDURE

The construction of each Bell state primarily involves rotating the half-wave plate within the quED set-up to change between diagonal and anti-diagonal polarization of the pumped blue photons to create the Triplet and Singlet states respectively. The rotation of the wave plate needs to be accounted for by repeating pointing alignment and beam-walking to improve visibility when each state is prepared. The correlation functions are calculated post-experiment, so the most care must be taken when connecting the beam-splitter either of the polarization-preserving fibers, the connection must remain between the end of the fiber coupler and fiber within the arm so the connection must be made directly on the quCR display. The Bell inequality measurement requires specific angles for maximal violation and can be safely automated on the quCR to get consistently precise orientations for the polarizers, but the calculations are better done manually as the quED cannot account for the flipping of the half-wave plate and automatically takes the absolute value.

VIII. RESULTS AND DATA ANALYSIS

VIII.A. Calculation of Correlation Function Values

For the detections between the two beam splitter outputs, we expect the photons entering the fiber coupler to be anti-bunched, that only a single photon arrives at the beam-splitter component and would result in being transmitted to channel 1 or reflected to channel 2. Resulting in no coincidence due to the indivisible nature of the photons as it only is incident on one of the detectors in the time window (Δt_w), also resulting in a correlation $g^{(0)}(\tau) = 0$. However, the imperfect nature of the system compared to our ideal case in the theory section, we detect more than 0 and our calculated correlation based on the counts is as follows in Table 2. The experimental results should not be very surprising as they support the expectation that the SPDC source is quite bunched is barely within the quantum regime. Additionally, the results are higher than 0 in the ideal case because we have additional photons from stray sources of light and from the dark counts of the detector, which is independent of the behavior of the input light.

$$g^{(2)}(\tau = 0) = \frac{N_{01} = 72}{(N_0 = 44249)\,(N_1 = 42117)} \frac{T = 1s}{\Delta t_w = 30ns} = 1.287$$

Table II: The singles and coincidence counts for regular correlation function

Trials	N_0	N_1	N_{01}	$g^{(2)}(0)$
1	44249	42117	72	1.287
2	44048	42442	60	1.069
3	44298	42350	47	0.835
4	44259	42198	59	1.053
5	43916	42099	56	1.009
6	44009	42495	50	0.891
7	43942	42105	59	1.062

With an integration set to default at 1 s, Multiple trials were taken to calculate the mean g value and the error. Therefore, $g^{(2)}(0) = 1.03 \pm 0.145$

For the heralded case, where the correlation where we are assured that the SPDC counts will be closer to a single photon source, we must consider 3-fold coincidences between all three detectors, we are guaranteed to have a single photon entering the beam splitter only if we detect a photon registered on the detector arm without any extra apparatus because the down-conversion process creates a pair of photons. Therefore, the correlation is as follows in Table 3 where the results match the expectation because the use of a detector arm as a trigger ensures that the SPDC is now a "heralded" single photon source and produces anti-bunched photons to better calculate the heralded correlation function.

$$g_H^{(2)}(\tau = 0) = \frac{(N_{012} = 2)\,(N_2 = 40491)}{(N_{02} = 348)\,(N_{02} = 363)} = 0.641$$

Table III: The singles and coincidence counts for heralded correlation function

Trials	N_2	N_{02}	N_{12}	N_{012}	$g_H^{(2)}(0)$
1	40491	348	363	2	0.641
2	40154	363	395	0	0
3	40538	320	408	0	0
4	40566	339	389	0	0
5	40407	365	386	0	0
6	40480	398	391	1	0.26
7	40997	353	384	0	0
8	40584	396	404	1	0.25

After including the beam-splitter and accounting for the detections condition on the trigger arm, the resulting $g_H = 0.143 \pm 0.23$

From the experimental calculation, it was apparent now that there may be sufficient trials to obtain an accurate reading statistically but it was known during the experimentation that the integration time to measure the coincidences could be increased beyond 1 second. The larger integration time with the same number of trials may have yielded better calculation for the regular correlation function as the small integration time could mistake coincidences for dark counts or stray light being detected within the finite detection window.

VIII.B. Triplet State

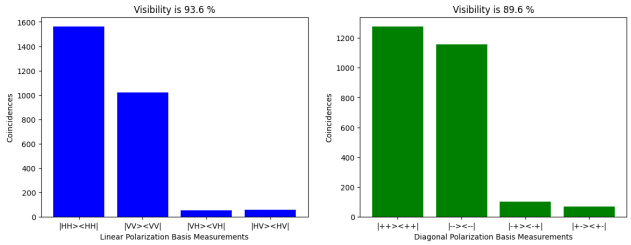

Fig. 11: The visibility of the Triplet State after optimization and calibration to prove that we are working with the correct state before Triplet state Bell's inequality

As described, the state is high in visibility in both bases of measurement and the alignment process was repeated several times to ensure the counts in the diagonal basis were highest for the $|PP\rangle$ and $|MM\rangle$ state as those are the expected states when re-writing the state from HV basis to PM basis using the Poincaré sphere in Fig 1. High visibility ensures that the state that is prepared is not mixed and is closest to the desired Bell state. In an ideal case, the counts on the other basis would be 0 and the visibility would be 100 %.

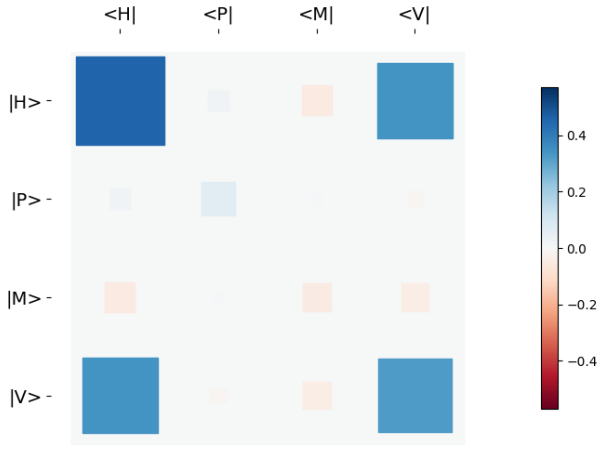

Fig. 12: Density Matrix of the Triplet State to illustrate that the Fidelity of the state is not perfectly in $|\Phi^+\rangle$ state, as the fidelity is 0.93

In addition, creating a density plot is helpful as the two-qubit tomography will be a better indicator if the state is maximally entangled as expected, as seen from the single qubit tomography, we get a mixed state with equal probability and doesn't give us enough information of the individual polarizations of the whole state.

Table IV: Coincidences for CHSH Inequality for Triplet State (ψ_s)

Pol. 1 ($\theta°$)	Pol. 2 ($\theta°$)	Rate 1	Rate 2	Coincidences
0.0	22.5	29407	24395	1078
0.0	67.5	28891	20096	208
0.0	112.5	29121	18874	164
0.0	157.5	30110	23719	1048
45.0	22.5	31081	24144	606
45.0	67.5	30990	20335	520
45.0	112.5	31296	19070	300
45.0	157.5	31123	23332	470
90.0	22.5	33301	24340	128
90.0	67.5	33123	20399	611
90.0	112.5	33345	19027	556
90.0	157.5	33142	23588	106
135.0	22.5	32360	24713	530
135.0	67.5	32195	20185	307
135.0	112.5	31954	18946	507
135.0	157.5	32193	23641	632

The coincidence measurements for all the expectation values for the total spin operator $\langle\psi_s|S|\psi_s\rangle$. The color coding represents the four expectation values that are as follows E_1 , E_2 , E_3 , E_4 .

Next doing the CHSH measurements, Table 4 shows the list of the combinations of $\alpha(\alpha')$ and $\beta(\beta')$ that are going to be the observations done by each of the detectors. The specific angle choices as explained in the theory result in maximal violation of the inequality. The color coding process is to obtain the four observibles that make up the inequality measurement which is the expectation of the total spin operator $\langle\psi_t|S|\psi_t\rangle$. The individual expectations value process is seen in Eqn 7 where the matching rows of data are counts of the angles for all terms. The resulting expectation values, however, are not the same as the Eqn 6. The Triplet state results in maximum contrast for the counts at a different set of measurements than the Singlet state as explained. This means that the signs for the four E terms are different for the triplet state resulting in Eqn 9. Finally, using Eqn 9 and Eqn 8, we can also calculate the expectation with the error.

$$\langle\psi_t|S|\psi_t\rangle = -E_1 + E_2 - E_3 + E_4 \tag{9}$$

$$\langle S\rangle = 2.516 \pm 0.038 \tag{10}$$

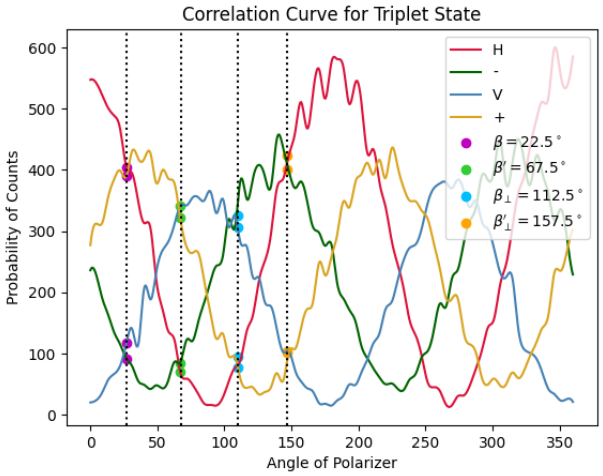

Fig. 13: The correlation curves along with the measurements for the CHSH inequality are marked, these are the chosen angles for the polarizers for measurements as the counts match for two bases, and for each of the four $\langle E \rangle$, the counts match another polarization measurement

To visualize maximum violation, the correlation curves are plotted to show the variety of angle combinations between the two detection arms that can be used to test Bell's inequality. The four main bases of polarization measurement are only phase-shifted as expected because the visibility was high enough to ensure coincidences were successfully detected. The location of the CHSH measurements is also labeled with the scattered plots along the dashed line which is where the correlation curves merge to two points instead of four and also have the largest contrast in coincidence counts as expected from Eqn 7. Each of the dashed lines represents an angle orientation for the second polarizer alone for each of the E values and a dot in a given dashed line would be one of the terms that make up one E value in Eqn 7. The accuracy of the marking of the CHSH measurements is relatively good as we can see the dot plots almost coincide to be two dots and are located almost exactly on the dashed line. This assures that the inequality is calculated accurately and that the state is maximally entangled despite the correlation curve sampling on 80 steps of angles between 0 and 360 degrees.

VIII.C. Singlet State

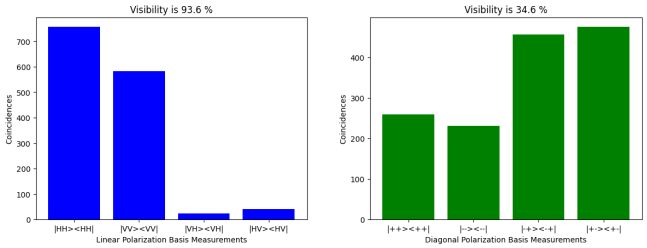

Fig. 14: This is the visibility for the Singlet state with very high counts registering in the $|PM\rangle$ and $|MP\rangle$ basis as the state re-written in diagonal basis as seen above shows what we expect. However, the visibility is still poor as there are too high counts in the $|PP\rangle$ and $|MM\rangle$ basis indicating that it is not a perfect $|\Phi^+\rangle$ state compared to the visibility of the Triplet state

As detailed in the caption Fig 12, shows that despite the best re-calibrations and alignment of the mirrors, there is some spatial mismatching that favors higher counts in $|PP\rangle$ and $|MM\rangle$ basis. This mismatching occurs within the SPDC set-up between the two BBO crystals and cannot be corrected without complete re-alignment or correction of the birefringent optical components. The higher counts in those basis indicates that the state is not very pure and another entangled state is interfering with our singlet state resulting in a poor fidelity of 0.71 for $|\Phi^-\rangle$ state.

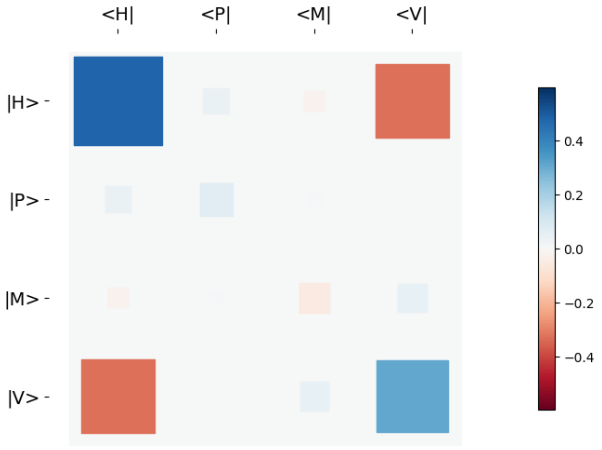

Fig. 15: This is the density plot of the Singlet state calibration, the state is not perfect as the fidelity of the state with the $|\Phi^+\rangle$ is only 71%. This result is supported by the previous figure showing poorer visibility because the state is mixed with higher counts in $|PP\rangle$ and $|MM\rangle$ when it should be lower for the pure state expected for $|\Phi^+\rangle$

Just as the triplet state, the density plot is more indicative of the purity of the state and we can see an imbalanced probability favoring the $|HH\rangle$ state more than the $|VV\rangle$ state.

Table V: Coincidences for CHSH Inequality for Singlet State (ψ_t)

Pol. 1 ($\theta°$)	Pol. 2 ($\theta°$)	Rate 1	Rate 2	Coincidences
0.0	22.5	26574	32583	878
0.0	67.5	26752	25801	145
0.0	112.5	26756	24242	184
0.0	157.5	26660	29884	920
45.0	22.5	30472	32854	152
45.0	67.5	30537	26261	191
45.0	112.5	30286	24280	623
45.0	157.5	30170	30058	646
90.0	22.5	35078	32871	147
90.0	67.5	34948	26198	593
90.0	112.5	34923	24081	544
90.0	157.5	35018	29837	92
135.0	22.5	31631	32755	674
135.0	67.5	31766	26196	595
135.0	112.5	32038	24201	97
135.0	157.5	31605	29920	234

The coincidence measurements for all the expectation values for the total spin operator $\langle\psi_t|S|\psi_t\rangle$. The color coding represents the four expectation values that are as follows E_1 , E_2 , E_3 , E_4 .

Following the similar color-coding process as the Triplet state, the total spin operator expectation is described in Eqn 6, and along with Eqn 8, Eqn 11 is the inequality measurement along with the error. If the error is included for our consideration, the state just about fails to violate Bell's inequality due to the mixedness of the state and more classical forces at play.

$$\langle S\rangle = 1.71 \pm 0.03 \tag{11}$$

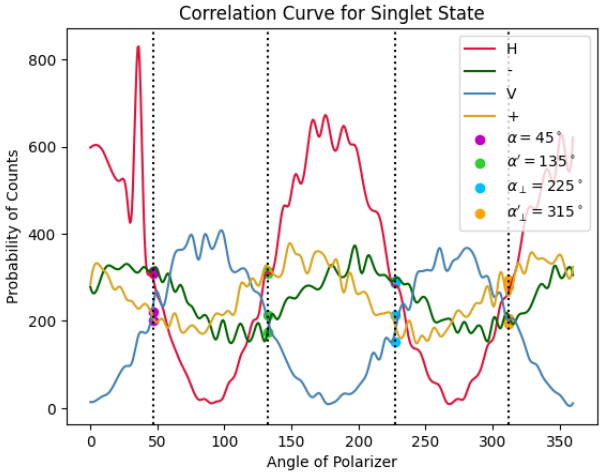

Fig. 16: The is the correlation curve for Singlet State

Fig 14 shows how the contrast for the different polarization measurements is significantly poorer because of the low visibility in the diagonal basis, therefore the line plot for the $|P\rangle$ orientation and $|M\rangle$ does not result in maximum contrast. The scatter plot of the CHSH measurement points does not align correctly with the dotted line and doesn't converge to two dots that are spaced furthest apart. The angles labeled are for the first detector arms instead as the state is different and also mixed. This is because the combination of measurements for maximally violating the inequality is different from the Triplet case.

IX. CONCLUSION

For the tomography, the single qubit tomography destroys the beauty of the constructed pure and entangled Bell state resulting in a mixed density matrix that is not useful to describe the individual photon states. Two qubit tomography preserves the information and produces a pure density matrix that captures the entanglement of the Bell state in terms of its probabilities. The full tomography for the triplet state and the supposed singlet state reveals much of what we expect from the calculation for the $\langle S\rangle$ for both states. The singlet state was difficult to create and the images and the constructed density matrix in the color plot show the comparison between the ideal matrix and the obtained matrix. The way we calibrated the quED set-up was to ensure very high counts $|PM\rangle\langle PM|$ and $|MP\rangle\langle MP|$ basis. Therefore, visibility is always poor for the singlet state but significantly better for the triplet state. The Fidelity of the density matrix with $|\Phi^+\rangle$ state is very close to 1 for the Triplet state $|\psi_t\rangle$ while the highest fidelity of the density matrix with $|\Phi^-\rangle$ is 0.75 for the Singlet state $|\psi_s\rangle$. From these steps alone we were able to predict which state would violate maximally Bell's Inequality. Finally, the correlation curves for the triplet state have sufficient contrast showing how the angle of measurement of the CHSH inequality was at positions where the detected coincidence was at the highest contrast for maximum violation. The location was very close to the exact angles despite having data with only 80 steps for plotting the correlation curves. The single state on the other hand, evidently has a different set angles compared to the Triplet case where maximum inequality violation would happen, but the curves cannot sufficiently support that claim because the contrast was too low for the diagonal basis. After all, it was shown how low the visibility was in Fig 12. Additionally, the regular and heralded function confirm the hypothesis that the HBT set-up alone is insufficient to match the ideal case because the regular SPDC photons are very bunched the inclusion of the heralded correlation function calculation treats the SPDC as a single photon source with very high anti-bunching properties, matching the expected case.

[a)] Physics and Astronomy Department, UCLA

[1] Gordon Baym. The physics of hanbury brown–twiss intensity interferometry: from stars to nuclear collisions, 1998.
[2] Christophe Couteau. Spontaneous parametric down-conversion. *Contemporary Physics*, 59(3):291–304, July 2018.
[3] Daniel F. V. James, Paul G. Kwiat, William J. Munro, and Andrew G. White. Measurement of qubits. *Phys. Rev. A*, 64:052312, Oct 2001.
[4] G. Peruzzo and S.P. Sorella. Entanglement and maximal violation of the chsh inequality in a system of two spins j: A novel construc-

tion and further observations. *Physics Letters A*, 474:128847, June 2023.

Appendix A: Single Qubit State Tomography

The following defined function is a Python program that outputs the density matrix for a single qubit state. The testing of the code is based on ensuring the trace of the matrix is equal to 1 and that the purity of the matrix is less than 1.

```
def density_1q(h, v, p, m, r, l):
    T_z  = (h - v)/(h + v)
    T_y  = (r - l)/(r + l)
    T_x  = (p - m)/(p + m)
    T_0  = 1

    rho = Qobj(1/np.sqrt(2)*(T_0*qeye(2)
    + T_x*sigmax() + T_y*sigmay()
    + T_z*sigmaz())).unit()
    return rho
```

1. Two-qubit state tomography

The following function will output a density matrix of size 16 with an input of all 36 measurements for the highest accuracy with an overcomplete tomography. The 36 measurements are funneled into a T matrix or tomography matrix which converts the measurements to Pauli Basis and finally tensor product with a pair of sigma operations. For example, the zx basis has a sum of measurements that forms the 'N' counts matrix, which can be used for all the subsequent T matrices.

$$N_{zx} = h_1p_2 + h_1m_2 + v_1p_2 + v_1m_2 \tag{A1}$$

Simplifying, the T matrix directly in terms of the measurements from the input matrix,

$$T_{zx} = f_{hp} - f_{hm} - f_{vp} + f_{vm} \tag{A2}$$

$$\therefore \tag{A3}$$

$$T_{zx} = \frac{h_1p_2 - h_1m_2 - v_1p_2 + v_1m_2}{N_{zx}} \tag{A4}$$

Similarly, defining a different another T matrix, with different signs for the non-fully correlated elements of the main T matrix, is to uphold the constraint that without any optical elements $T_00 = 1$

$$T'_{zx} = \frac{h_1p_2 + h_1m_2 - v_1p_2 - v_1m_2}{N_{zx}} \tag{A5}$$

$$\therefore \tag{A6}$$

$$T_{z0} = \frac{1}{3}\left(T'_{zz} + T'_{zx} + T'_{zy}\right) \tag{A7}$$

$$T_{0y} = \frac{1}{3}\left(T'_{zy} + T'_{xy} + T'_{yy}\right) \tag{A8}$$

```
def density_2q(input):

  N = np.zeros((4,4))
  T = np.zeros((4,4))
  antT = np.zeros((4,4))

  for i in range(1,4):
    for j in range(1,4):
      N[i,j] = (input[2*i-2,2*j-2] + input[2*i-2,2*j-1]
      + input[2*i-1,2*j-2] + input[2*i-1,2*j-1])
      T[i,j] = (input[2*i-2,2*j-2] - input[2*i-2,2*j-1]
      - input[2*i-1,2*j-2] + input[2*i-1,2*j-1])/N[i,j]
      antT[i,j] = (input[2*i-2,2*j-2] + input[2*i-2,2*j-1
      - input[2*i-1,2*j-2] - input[2*i-1,2*j-1])/N[i,j]

  for i in range(1,4):
    T[i,0] = 1/3 * (antT[i,1] + antT[i,2] + antT[i,3])
    T[0,i] = 1/3 * (antT[1,i] + antT[2,i] + antT[3,i])
    T[0,0] = 1

  sigma = [identity(2), sigmaz(), sigmax(), sigmay()]
  temp = []
  for i in range(4):
    for j in range(4):
      temp.append(T[i,j] * np.kron(sigma[i], sigma[j]))

  density = 1/4*Qobj(reduce(add, temp))
  return density
```